nature communications

Article

https://doi.org/10.1038/s41467-024-54321-y

Synthesis and redox catalysis of Carbodiphosphorane ligated stannylene

Received: 9 May 2024

Accepted: 5 November 2024

Published online: 14 November 2024

Check for updates

Zhuchunguang Liu[1,2], Zhijun Wang[1,2], Huan Mu[1], Yihan Zhou[1], Jiliang Zhou[1] & Zhaowen Dong[1]

Heavier group 14 carbene analogues, exhibiting transition-metal-like behavior, display remarkable capability for small molecule activation and coordination chemistry. However, their application in redox catalysis remains elusive. In this paper, we report the synthesis and isolation of a stannylene with carbodiphosphorane ligand. The nucleophilic reactivity at the divalent tin center is elucidated by computational and reactivity studies. Moreover, this stannylene exhibits catalytic activity in the hydrodefluorination reaction of fluoroarenes. Mechanistic investigations into the elementary steps confirm a Sn^{II}/Sn^{IV} redox cycle involving C–F oxidative addition, F/H ligand metathesis, and C–H reductive elimination. This low-valent Sn^{II} catalytic system resembles the classical transition metal catalysis. Notably, this represents metallomimetic redox catalysis utilizing carbene analogue with heavier group 14 element as a catalyst.

Carbenes and their heavier group 14 analogues are at the forefront of modern main group chemistry because their unique electron configuration, featuring a vacant *p*-orbital and a lone pair of electrons, allows them to act as both electron donors and electron acceptors (Fig. 1B)[1–11]. These amphiphilic species have the potential to mimic the behavior of transition metals, thus offering an effective alternative to transition metal catalysis[12]. In the past two decades, research on the carbene analogues has primarily focused on their synthesis and reactivity[5–11]. However, their application in redox catalysis remains elusive. Unlike transition metals that readily engage in redox catalysis by shuttling between different oxidation states (Fig. 1A), carbene analogues face challenges in the subsequent reductive elimination from the high valence state after oxidative addition, thereby impeding the completion of the catalytic cycle (Fig. 1B)[13–17]. Despite significant achievements in bridging the gap between bond activation and catalysis, achieving simple redox catalysis using carbene analogues as catalysts seems still within sight but beyond reach.

Over the last decade, it has been recognized that geometric perturbation serves as an effective strategy for fine-tuning the electronic configuration of the main group elements[18,19]. This approach has unlocked the unique reactivity and catalytic potential in main group compounds. Recent studies indicate that the utilization of multidentate pincer ligands leads to the formation of the deformed pnictogen compounds, thereby imparting them with characteristics of transition metals[18–22]. These geometrically constrained pnictogen systems have demonstrated their ability to act as catalysts in redox catalysis via P^{III}/P^{V} or Bi^{I}/Bi^{III} redox cycles[20,21]. Remarkably, these catalytic systems involving group 15 elements exhibit all three fundamental steps consisting of oxidative addition (OA), ligand metathesis (LM) and reductive elimination (RE), which are pivotal to the transition metal catalytic mechanisms (Fig. 1A). The impressive advancements in geometrically constrained organopnictogen redox catalysis have refined the framework of main group catalysis. Cognizant of this, we propose that the ligand-enforcement strategy can endow heavier group 14 systems with distinctive properties, thereby facilitating the development of group 14 redox catalysts.

Herein, we report a stannylene **1** with nucleophilicity supported by the rigid carbodiphosphorane ligand (Fig. 1C). Reactivity studies demonstrate that stannylene **1** exhibits capability in activating σ-bonds via oxidative addition, while the corresponding adduct undergoes ligand metathesis in the presence of an additive. More importantly, stannylene **1** presents catalytic activity for facilitating the hydrodefluorination of fluoroarenes via C–F oxidative addition, F/H ligand metathesis, and C–H reductive elimination processes, akin to the

[1]Key Laboratory of Green Chemistry & Technology, Ministry of Education, College of Chemistry, Sichuan University, 610064 Chengdu, People's Republic of China. [2]These authors contributed equally: Zhuchunguang Liu, Zhijun Wang. e-mail: dongzhaowen@scu.edu.cn

https://doi.org/10.1038/s41467-024-54321-y

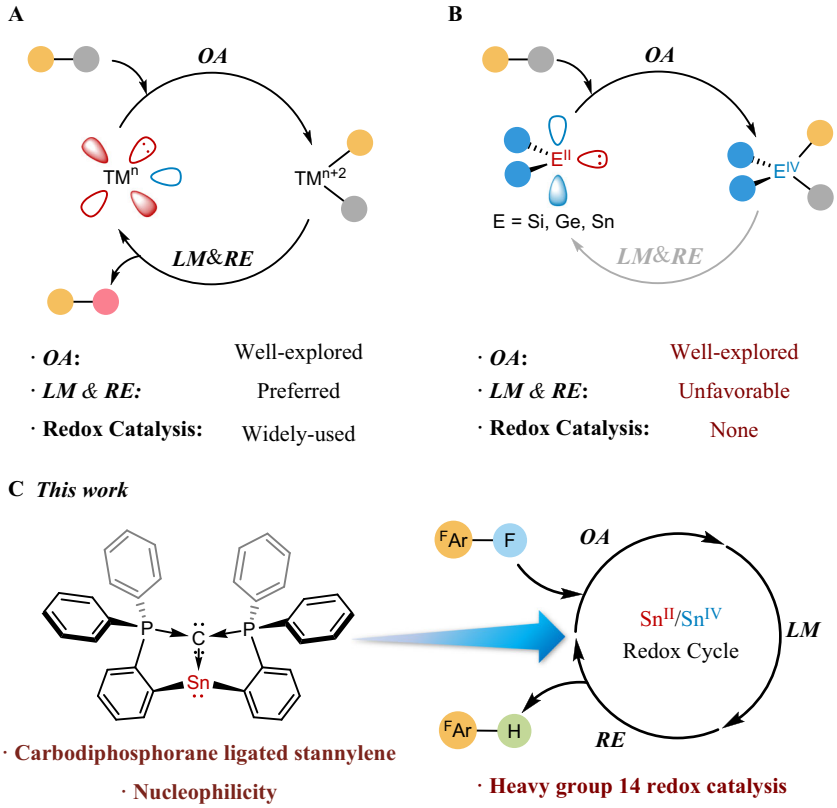

Fig. 1 | Redox catalysis with transition metal complexes or carbene analogues. **A** Well-studied transition-metal mediated redox catalysis. **B** TM-behavior of heavier group 14 carbene analogues and their potential application in redox catalysis. **C** Carbodiphosphorane ligated stannylene and its application as redox catalyst in the hydrodefluorination of fluoroarenes. TM transition metal, OA oxidative addition, LM ligand metathesis, RE reductive elimination.

classical transition metal catalysis. This represents an example of metallomimetic catalysis involving a Sn^{II}/Sn^{IV} redox cycle.

Results and discussion

Synthesis and characterization of the stannylene

Our study commenced with the preparation of carbodiphosphorane ligated stannylene **1**. The salt metathesis reaction between dilithiocarbodiphosphorane (Li_2CDP)[23–27] and stannous chloride in tetrahydrofuran (THF) at −30 °C resulted in the CDP stannylene (CDPSn) **1** as main product, which could be isolated in 71% yield (Fig. 2A). The identity of CDPSn **1** was initially demonstrated by nuclear magnetic resonance (NMR) spectroscopy. The product presents a low field ^{31}P NMR resonance ($\delta^{31}P = 24.1$ ppm) compared to what is found in the starting material Li_2CDP ($\delta^{31}P = 17.0$ ppm) (Table S5)[23]. A significantly high field signal in the ^{119}Sn NMR spectrum at 135.9 ppm is observed for the central tin atom verifying the product formation. Comparison with ^{119}Sn NMR chemical shifts of the general dicoordinated stannylene ($\delta^{119}Sn$ = ca. 2000–3000 ppm) indicates the coordination number of the central Sn atom in **1** is larger than two[28–32].

Yellow crystals of **1**, suitable for single crystal X-ray diffraction (sc-XRD) analysis, were obtained by slow diffusion of *n*-hexane onto a concentrated toluene solution of **1** at room temperature. The crystallographic analyses show that the tin atom adopts a tricoordinated environment with the sum of the bond angles around the tin atom Σα(Sn) = 269.0°, implying the presence of a lone pair at the tin atom (Fig. 2B). The two five-membered Sn-heterocycles form a butterfly confirmation with a dihedral angle of θ = 71°. Attributable to the rigidity of the trident pincer-type CDP ligand, stannylene **1** is forced into a C_s type geometry, which is distinct from the reported carbodiphosphorane-$GeCl_2$ complex ($(Ph_3P)_2C{-}GeCl_2$) with a regular C_{3V} geometry[33]. The inner-cyclic Sn–C1 bond length (2.278(2) Å) is somewhat longer than the Sn–C2 and Sn–C3 bonds (2.254(2) Å, 2.219(2) Å) and those in diaryl/dialkyl stannylene (2.20–2.27 Å)[28–31]. However, it is shorter than the $C_{NHC} \rightarrow Sn$ dative bond in the N-heterocyclic carbene (NHC) stabilized stannylene (Sn–C_{NHC}: 2.29–2.33 Å) (Table S4)[34,35]. These results confirm the expected bonding situation of σ-donation of the C1 atom into the vacant 5p-orbital of the central tin atom. Overall, the Sn–C1 bond in **1** may be described with a resonance between dative bond and electron-sharing σ-bond (Fig. 2A).

To further elucidate the electronic situation of CDPSn **1**, density functional theory (DFT) calculations were performed at the BP86-D3(BJ)/def2-TZVP level[36]. The highest occupied molecular orbital (HOMO) in **1** consists of a lone pair ($sp^{0.27}$ hybrid), indicating its nucleophilic character, which is consistent with the results of sc-XRD analysis (Fig. 2C). Electron localization function (ELF) calculations were carried out for **1** (Fig. 2D)[37]. The presence of the red region at the bottom-right of the Sn atom again validates the presence of a lone pair on Sn atom. Furthermore, we performed the quantum theory of atoms in molecules (QTAIM) analysis to gain further details for the bonding nature between Sn atom and C1 atom in **1**[38]. The contour plot of the Laplacian of electron density ($\nabla^2\rho(r)$) in the C1–Sn–C2 plane is shown in Fig. 2E. The results of QTAIM analysis disclose that the Sn–C1 bond in **1** can be classified as typical donor–acceptor bond with its bond critical point (BCP) located proximally to a nodal surface of the Laplacian $\nabla^2\rho(r)$ and a negative value for the total energy density $H(r_c)$. For standard single bond, the ellipticity value ($\varepsilon(r_c)$) should be zero due to the cylindrical contour of electron density. In the case of **1**, the ellipticity value ($\varepsilon(r_c)$ = 0.03) for Sn–C1 bond is close to zero, pointing out the absence of donation of π lone pair of C1 atom to Sn atom. These observations were further supported by natural bond orbital (NBO) analysis[39], where the Sn–C1 σ-bond and the π-lone pair on C1 atom were

https://doi.org/10.1038/s41467-024-54321-y

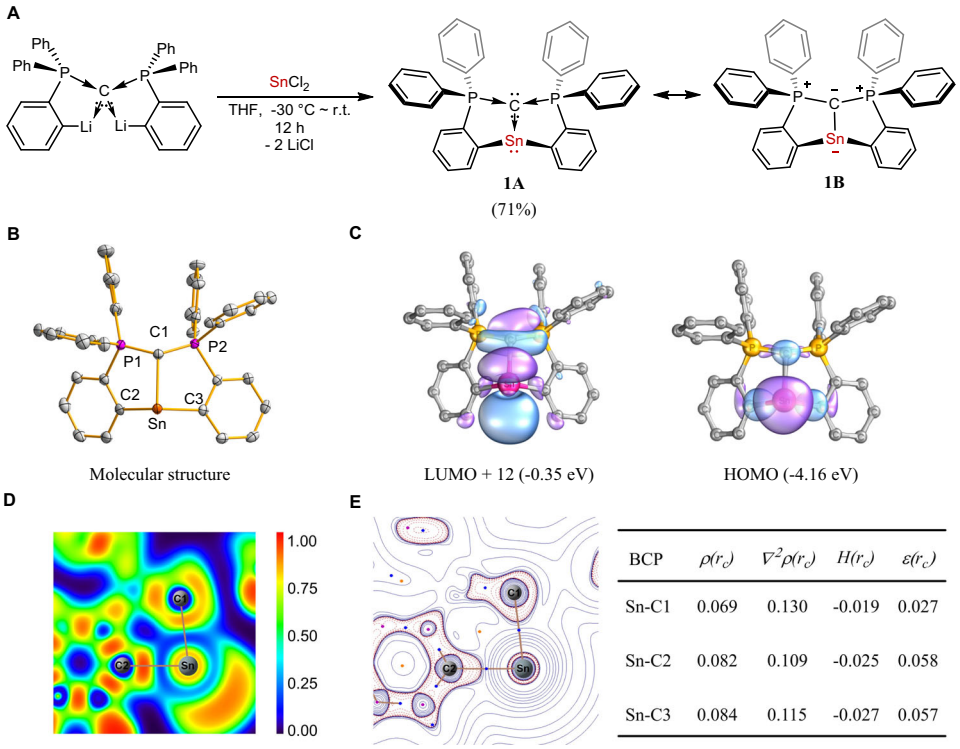

BCP	$\rho(r_c)$	$\nabla^2\rho(r_c)$	$H(r_c)$	$\varepsilon(r_c)$
Sn-C1	0.069	0.130	-0.019	0.027
Sn-C2	0.082	0.109	-0.025	0.058
Sn-C3	0.084	0.115	-0.027	0.057

Fig. 2 | The synthesis and computational analysis of stannylene 1. A Synthetic approach of stannylene **1**. **B** Molecular structure of **1** in the solid state (Hydrogen atoms and solvent molecules are omitted for clarity. Thermal ellipsoids are at the 50% probability level). **C** Selected frontier molecular orbital of **1**. **D** Electron localization function analysis of C1–Sn–C2 plane in **1**. **E** The contour plot of the Laplacian of electron density ($\nabla^2\rho(r_c)$) in the C1–Sn–C2 plane of **1**. BCP: bond critical point; $\rho(r_c)$: electron density; $\nabla^2\rho(r_c)$: Laplacian of electron density; $H(r_c)$: total electron energy density; $\varepsilon(r_c)$: ellipticity of electron density. All computational analysis was calculated at the BP86-D3(BJ)/def2-TZVP level.

identified and the Wiberg bond index (WBI)[40] value of 0.51 for Sn–C1 bond fell into the typical range of C→Sn dative bond (Fig. S90)[34,35]. On the basis of these computational findings, two major resonance structures of **1** are described in Fig. 2A, consistent with the results of the structural and spectroscopic analyses.

Reactivity studies of the stannylene

Stannylenes have been extensively studied in transition metal coordination and bond activation chemistry[5–11,14–17]. To examine the reactivity of stannylene **1**, we next investigated its reactions with $Fe_2(CO)_9$, methyl iodide and pentafluoropyridine (Fig. 3). **1** reacted smoothly with $Fe_2(CO)_9$ in THF at room temperature to give complex **2** in 81% yield, which was fully characterized by NMR, sc-XRD analysis and infrared (IR) spectroscopy. The shielded ^{119}Sn resonance (342.7 ppm) is observed in ^{119}Sn NMR spectrum of iron complex **2** in comparison with that in **1** (135.9 ppm) (Table S5). The Sn–Fe bond (2.530(7) Å) in **2** is characteristic for a typical Sn–Fe single bond (2.50–2.65 Å)[32]. The infrared bands of the CO groups in **2** are important parameters for evaluating the donor ability of stannylene **1**[41]. The A_1 CO stretching frequency at $\nu_{CO} = 2004\ cm^{-1}$ of **2** is smaller than the isostructural $Fe(CO)_4$ complexes of $^tBu_3P$ ($\nu_{CO} = 2045\ cm^{-1}$), and N-heterocyclic carbenes (NHC) ($\nu_{CO} = 2035–2037\ cm^{-1}$). This demonstrates the σ-donating property of CDPSn **1** is stronger than the $^tBu_3P$ and NHC ligands. The significantly strong donor property was re-corroborated by calculating the ν_{CO} of the model [CpIr(CO)L] complex described by Gusev (see Supplementary Information, Table S7)[42].

Studies in σ-bond activation were subsequently investigated by the reaction of **1** with CH_3I or pentafluoropyridine. After workup, adducts **3** and **4** were isolated in yields of 80% and 17% respectively. The ^{119}Sn NMR signals (−36.1 and −172.1 ppm) for tin atoms of **3** and **4** shift to the up-field in comparison with those in **1** (135.9 ppm) and **2** (342.7 ppm). The C1–Sn bond distances in **3** (2.215(2) Å) and **4** (2.240(3) Å) are approximately the same as those found in **1** (2.278(2) Å) and **2** (2.200(3) Å) (Fig. 3B and Table S4). Interestingly, when the LiCl was added as an additive into the THF solution containing **4**, the white participation **5** was obtained via Cl/F ligand exchange. A simple one-pot preparation of **5** could be achieved via the treatment of **1** with pentafluoropyridine and LiCl. The structural parameters of **5** are very close to what were found for **4** (for details, see Table S4). Under the condition that oxidative addition and ligand metathesis can proceed smoothly, **1** shows the possibility to break through the boundaries between small molecular activation and chemical bond formation. Therefore, we contemplated the feasibility of employing **1** as catalyst for redox catalytic reactions.

Redox catalysis of the stannylene

Inspired by the pioneering work of Radosevich, Cornella, et al.[27,43–45] on organopnictogen-mediated catalytic hydrodefluorination (HDF), this unsophisticated yet meaningful reaction was chosen as a template reaction to shed light on the application of **1** in redox catalysis. The HDF of pentafluoropyridine (**6a**) with $PhSiH_3$ is selected as our prototypical system. We were surprised to discover that CDPSn **1** did catalyze the HDF of **6a** (Fig. 4A). A variety of reaction conditions were examined to explore the effects of stannylene, silane, solvent and temperature on the HDF of **6a** (For detail, see Table S1–2). Systematic screening of reaction conditions led to the identification of optimal conditions as follows: 0.4 equiv. of $PhSiH_3$ and 10 mol% of CDPSn **1** in THF at 60 °C for 2 h. Under the conditions, the desired product 2,3,5,6-tetrafluoropyridine **7a** was obtained in almost quantitative yield. To the best of our knowledge, this is catalytic HDF reaction using a low-valent stannylene as the catalyst.

The studies then segued to investigate the reaction mechanism after confirming the feasibility of catalytic HDF using **1** as catalyst. The plausible mechanism is depicted in Fig. 4A. The reaction initiates with

https://doi.org/10.1038/s41467-024-54321-y

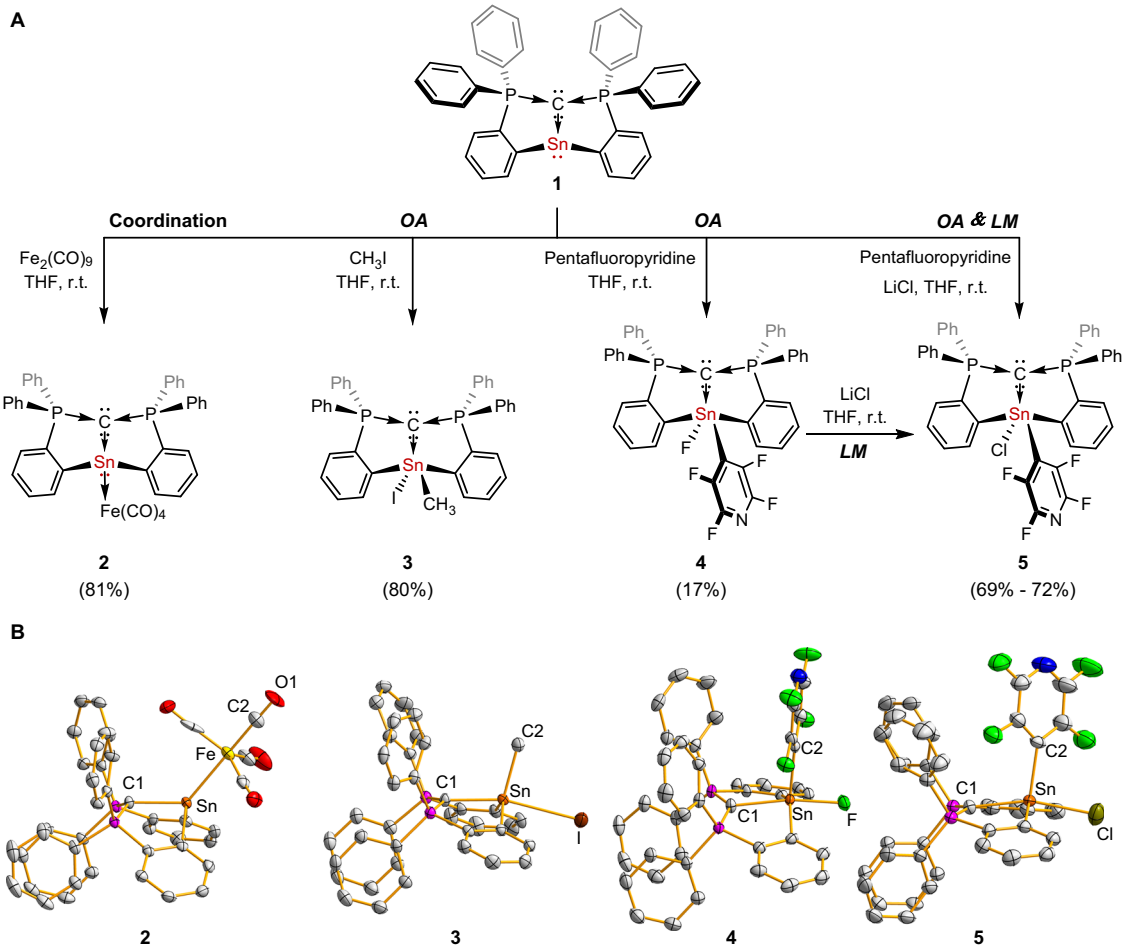

Fig. 3 | Reactivity studies of 1. A Reaction of **1** with $Fe_2(CO)_9$ gave complex **2**. Oxidative addition reaction of **1** with CH_3I and pentafluoropyridine afforded adducts **3** and **4**. Compound **5** was formed via ligand metathesis of **4** with LiCl, or via a one-pot reaction by combining **1**, pentafluoropyridine and LiCl. **B** Molecular structures of **2**–**5** in the solid state (Hydrogen atoms and solvent molecules are omitted for clarity. Thermal ellipsoids are at the 50% probability level).

the oxidative addition between nucleophile **1** with **6a** through a stepwise pathway intermediated by Meisenheimer complex **8**[46], resulting in the Sn^{IV} intermediate **4**. Then the hydrosilane **A** reacts smoothly with **4** to afford Sn–H species **9** via ligand metathesis along with the formation of fluorosilane **B**. The subsequent reduction elimination of **9** leads to catalyst turnover and finally delivers product **7a**.

The process for the formation of intermediate **4** via oxidative addition of **1** with **6a** was well-defined, as mentioned earlier for the reactivity studies of **1** (Fig. 3). To shed light on the ligand metathesis and reductive elimination processes, the in-situ reaction between Sn^{IV} compound **4** and $PhSiH_3$ (1.0 equiv.) in THF-d_8 was investigated by NMR spectroscopy at different time intervals (Figs. S2–4). After 5 min, a high field signal at 10.8 ppm (blue labeled) was observed in the ^{31}P NMR spectrum along with the distinctively diminished signal at 13.4 ppm (green labeled) of **4**, which unambiguously validated the formation of Sn^{IV} intermediate **9** via F/H ligand metathesis (Fig. 4B). The green labeled signal disappeared completely 30 min later, demonstrating that the F/H ligand metathesis reaction could finish in a short time. The subsequent reductive elimination process resulted in the generation of the catalyst CDPSn **1** detected by the ^{31}P NMR spectroscopy ($\delta^{31}P = 24.1$ ppm, red labeled). The complete transformation from **9** to **1** requires approximately 12 h, which is considerably longer than oxidative addition (within 5 min) and ligand metathesis (within 30 min) processes, indicating that reductive elimination is the rate-limiting step in HDF of **6a**. Further evidence supporting the formation of **9** via ligand exchange was obtained by high-resolution mass spectrometry (HRMS) (Fig. S5) and ^{19}F NMR spectroscopic analysis (Fig. S3). The triplet ^{19}F NMR resonance at $\delta^{19}F = -171.6$ ppm, assigned to the F atom bonding with Sn atom in **4**, disappeared within 5 min after the addition of $PhSiH_3$, revealing that the reaction between the **4** and $PhSiH_3$ was conspicuous (Fig. S3). The generation of **9** was also detected via ^{19}F NMR in which F atoms resonate at −97.4 and −124.5 ppm respectively.

To further understand the reaction mechanism, DFT calculations were performed on the potential energy surface (PES) of the reaction at the theoretical level of BP86-D3(BJ)/def2-TZVP (Fig. 4C). The computational results indicate that the oxidative addition of Sn^{II} in **1** to the C–F bond can be accomplished with thermodynamic favorableness, involving energy barriers of $\Delta G^{\ddagger} = 9.0$ kcal/mol for the formation of a Meisenheimer-type intermediate **8** and facile fluoride migration to afford intermediate **4** ($\Delta G^{\ddagger} = 0.3$ kcal/mol). This process is a stepwise nucleophilic aromatic substitution (S_NAr) reaction leading to the initial Sn–F formation[46]. Subsequently, $PhSiH_3$ participates in the ligand metathesis of the Sn–F bond, proceeding through a four-membered ring transition state **TS3** and overcoming an energy barrier of $\Delta G^{\ddagger} = 16.9$ kcal/mol to reach the hydride intermediate **9**. Finally, a reductive elimination step leads to the release of the product and regeneration of catalyst **1**. It is noteworthy that reductive elimination is the rate-determining step of the reaction ($\Delta G^{\ddagger} = 25.3$ kcal/mol), which is consistent with experimental results. Other possible mechanistic pathways (e.g. single electron transfer[47]) were also investigated and discussed in view of the computed energy profile (see Supplementary Section 2.4.7). The energy barriers for the alternative mechanisms are all higher than the proposed mechanism (shown in Fig. 4C) involving

https://doi.org/10.1038/s41467-024-54321-y

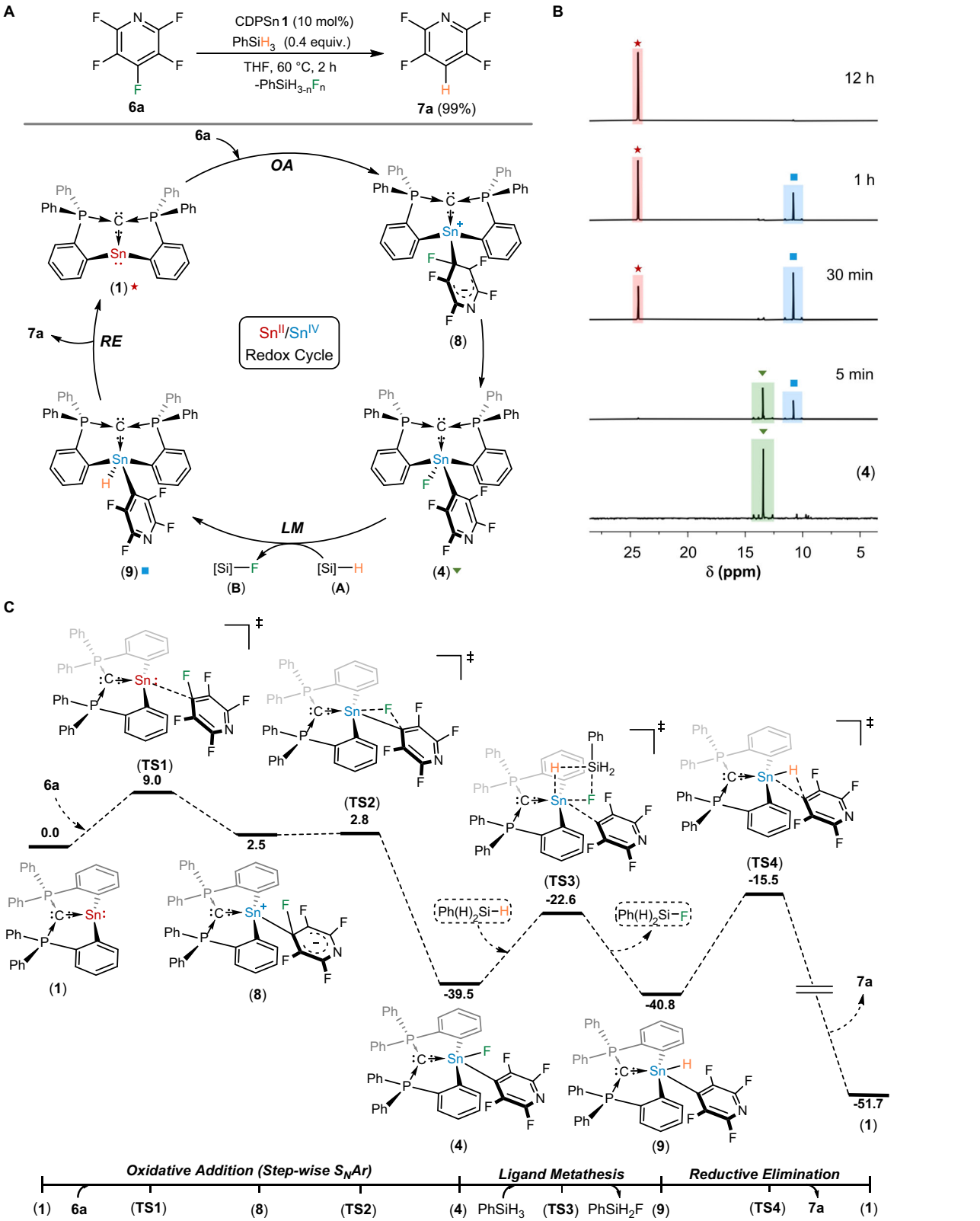

Fig. 4 | Mechanism studies for Sn^{II}-catalyzed hydrodefluorination of pentafluoropyridine. A Proposed catalytic cycle of HDF reaction. **B** Overlay of ^{31}P NMR spectra (THF-d_8, 162 MHz, argon atmosphere, room temperature.) of the reaction of **4** with $PhSiH_3$ (1.0 equiv.) recorded at variable time. **C** The calculated potential energy surface of the catalytic cycle of HDF reaction (in kcal/mol). The free energy was obtained at the theoretical level of BP86-D3(BJ)/def2-TZVP/THF(IEFPCM)//BP86-D3(BJ)/def2-SVP/THF(IEFPCM).

https://doi.org/10.1038/s41467-024-54321-y

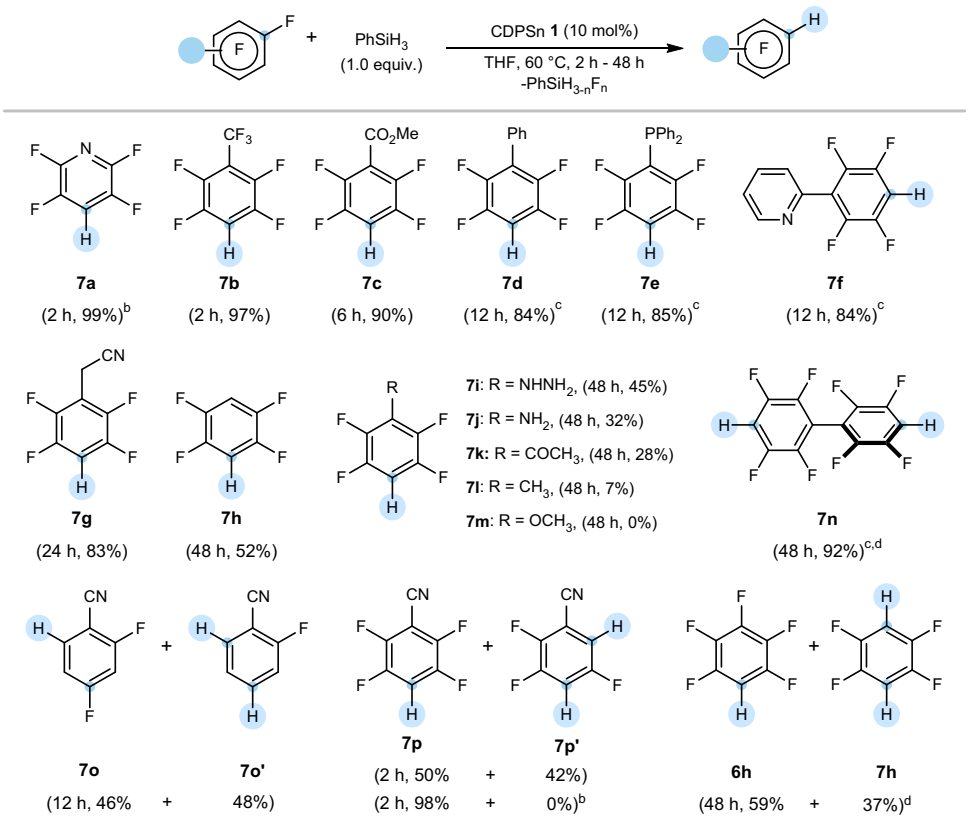

Fig. 5 | Scope of the catalytic hydrodefluorination of fluoroarenes. Reactions were performed on a 0.25 mmol scale; Reaction time and yields were reported in parentheses. Yields were calculated by quantitative ^{19}F NMR using 4-fluorotoluene as internal standard, unless stated otherwise. [a]In the presence of 0.4 equiv. of $PhSiH_3$. [b]Isolated yields. [c]In the presence of 2.0 equiv. of $PhSiH_3$.

C–F oxidative addition, F/H ligand metathesis, and C–H reductive elimination.

With an in-depth comprehension of the mechanism of CDPSn **1**-catalyzed HDF reaction, the substrate scope of the HDF was tested under the optimized reaction conditions (Fig. 5). The scope of the catalytic HDF reaction includes pentafluoropyridine **6a** and other fluoroarenes with distinct electronic properties. Pentafluorobenzenes bearing electron-withdrawing or electron-neutral groups were all well-tolerated, affording the desired para-hydrogenated products **7b**–**7g** in high yields (84%–97%) and with high selectivity. The HDF of pentafluorobenzenes with formyl group or electron-donating group could also proceed under the standard condition (**6h**–**6k**), delivering the hydrodefluorinated products in diminished yields (28–52%). For pentafluorotoluene **6 l** and pentafluoroanisole **6 m** with stronger electron-donating groups, however, only trace amounts of desired products were detected. Remarkably, the catalytic HDF required more time as the decrease of the electron-withdrawing abilities of the substituents, confirming the significant effect of the electronic properties of the substrates on the reaction. Reactants with multiple active sites were also within the scope of the investigation. Excessive $PhSiH_3$ would lead to the diHDF of perfluorobiphenyl **6n**, 2,4,6-trifluorobenzonitrile **6o**, 2,3,4,5,6-pentafluorobenzonitrile **6p** and hexafluorobenzene **6q**, giving the corresponding mono- or double-hydrogenated products in moderate to good yields. Partially fluorinated substrate **6o** proved to be a reliable substrate, producing the mixture of 2,4-difluorobenzonitrile **7o** (46%) and 2-fluorobenzonitrile **7o'** (48%). Furthermore, the selectivity of the products in the HDF reaction of **6p** could be controlled by altering the amount of $PhSiH_3$. Compared to previous pnictogen systems[27,44,45], catalyst **1** showed better performance in the case of substrates with weak electron-donating groups (**6i, 6j**) and non-perfluorine substitutes (**6o**). These findings disclose that the functional groups are generally tolerated in Sn^{II}-catalyzed HDF reaction, and again highlight the feasibility of employing stannylene **1** as surrogates of transition metal catalyst in redox catalysis.

Ever since Power's groundbreaking review on the concept of "Main-group elements as transition metals", the group 14 carbene analogues have been central for main group chemistry[12]. However, the application of these low-valent species in redox catalysis remains elusive due to the inherent challenges associated with achieving the E^{II}/E^{IV} (E = Si, Ge or Sn) catalytic cycle. Herein, we have reported the synthesis and isolation of a nucleophilic stannylene **1** supported by the tridentate pincer carbodiphosphorane ligand. Stannylene **1** can function as a strong Sn-donor ligand, as demonstrated by the synthesis of iron complex. The observation of the oxidative addition and ligand metathesis processes during the reaction of **1** with pentafluoropyridine **6a** is particularly noteworthy, as it resembles elementary steps in transition metal redox catalysis. Furthermore, we have successfully achieved the catalytic HDF reaction using stannylene **1** as a redox catalyst, which undergoes sequential C–F oxidative addition, F/H ligand metathesis, and C–H reductive elimination processes. As yet, this is an example of main group catalysis involving Sn^{II}/Sn^{IV} redox couple. Currently, we are exploring further possibilities for applying the group 14 carbene analogues in various redox catalytic reactions.

Methods

Synthesis of stannylene 1

Stannous chloride (183 mg, 1.0 mmol, 1.0 equiv.) was added to a THF (15 mL) solution of dilithio-carbodiphosphorane (548 mg, 1.0 mmol) at −30 °C. The reaction mixture was allowed to warm to room temperature after 10 min and then stirred for 12 h to form a yellow solution. Subsequently, all the volatiles were removed under reduced pressure, and the resulting solid was washed with *n*-hexane (10 mL). The solid

was re-dissolved in toluene (30 mL) and the solution was filtered by using a PTFE syringe filter to remove LiCl. The solvent was removed in vacuum and the product **1** was obtained as yellow powder. Yield: 464 mg (71%). Bright yellow crystals, suitable for X-ray analysis, were obtained by slow diffusion of *n*-hexane onto a solution of **1** in toluene at room temperature.

General procedure for HDF

In a glovebox, stannylene **1** (14.0 mg, 0.02 mmol, 10 mol%) and THF (1.25 mL) were added to a Schlenk tube. The tube was taken out of the glovebox and charged with polyfluoroarenes (0.25 mmol), $PhSiH_3$ (0.4–2.0 equiv.) upon stirring. The reaction was carried out for different time at 60 °C. After completion of the reaction, the mixture was cooled to room temperature and exposed to air to quench the reaction. The product was isolated by flash chromatography. If product was volatile, 4-fluorotoluene (27.5 mg, 0.25 mmol, 1.0 equiv.) was used as internal standard and the product was analyzed by quantitative ^{19}F NMR.

Data availability

General information, experimental details, and analytical data: NMR spectra, HRMS data, IR spectrometry data and computational details can be found in the Supplementary Information. The X-ray crystallographic coordinates for structures reported in this study have been deposited at the Cambridge Crystallographic Data Centre (CCDC), under deposition numbers 2344193 (**1**), 2344194 (**2**), 2344195 (**3**), 2344196 (**4**) and 2344197 (**5**), respectively. These data can be obtained free of charge from The Cambridge Crystallographic Data Centre via www.ccdc.cam.ac.uk/data_request/cif. Source Data containing optimized Cartesian coordinates are provided in this paper. All data are available from the corresponding author upon request. Source data are provided with this paper.

References

1. Soleilhavoup, M. & Bertrand, G. Stable Carbenes, Nitrenes, Phosphinidenes, and Borylenes: Past and Future. *Chemistry* **6**, 1275–1282 (2020).
2. Nesterov, V. et al. NHCs in Main Group Chemistry. *Chem. Rev.* **118**, 9678–9842 (2018).
3. Doddi, A., Peters, M. & Tamm, M. N-Heterocyclic Carbene Adducts of Main Group Elements and Their Use as Ligands in Transition Metal Chemistry. *Chem. Rev.* **119**, 6994–7112 (2019).
4. Bellotti, P., Koy, M., Hopkinson, M. N. & Glorius, F. Recent Advances in the chemistry and applications of N-heterocyclic carbenes. *Nat. Rev. Chem.* **5**, 711–725 (2021).
5. He, M., Hu, C., Wei, R., Wang, X.-F. & Liu, L. L. Recent advances in the chemistry of isolable carbene analogues with group 13–15 elements. *Chem. Soc. Rev.* **53**, 3896–3951 (2024).
6. Duan, C. & Cui, C. Boryl-substituted low-valent heavy group 14 compounds. *Chem. Soc. Rev.* **53**, 361–379 (2024).
7. Wang, L., Li, Y., Li, Z. & Kira, M. Isolable silylenes and their diverse reactivity. *Coord. Chem. Rev.* **457**, 214413 (2022).
8. Asay, M., Jones, C. & Driess, M. *N*-Heterocyclic Carbene Analogues with Low-Valent Group 13 and Group 14 Elements: Syntheses, Structures, and Reactivities of a New Generation of Multitalented Ligands. *Chem. Rev.* **111**, 354–396 (2011).
9. Mizuhata, Y., Sasamori, T. & Tokitoh, N. Stable Heavier Carbene Analogues. *Chem. Rev.* **109**, 3479–3511 (2009).
10. Dong, Z., Albers, L. & Müeller, T. Trialkylsilyl-Substituted Silole and Germole Dianions as Precursors for Unusual Silicon and Germanium Compounds. *Acc. Chem. Res.* **53**, 532–543 (2020).
11. Dasgupta, R. & Khan, S. N-Heterocyclic germylenes and stannylenes: Synthesis, reactivity and catalytic application in a nutshell" in *Advances in Organometallic Chemistry* (Elsevier, 2020), pp. 105–152.
12. Power, P. P. Main-group elements as transition metals. *Nature* **463**, 171–177 (2010).
13. Baird, S. R. & Rivard, E. Narrowing the reactivity gap between transition metals and silicon for catalysis. *Chem* **10**, 1043–1045 (2024).
14. Chu, T. & Nikonov, G. I. Oxidative Addition and Reductive Elimination at Main-Group Element Centers. *Chem. Rev.* **118**, 3608–3680 (2018).
15. Hadlington, T. J., Driess, M. & Jones, C. Low-valent group 14 element hydride chemistry: towards catalysis. *Chem. Soc. Rev.* **47**, 4176–4197 (2018).
16. Weetman, C. & Inoue, S. The Road Travelled: After Main-Group Elements as Transition Metals. *Chem. Cat. Chem.* **10**, 4213–4228 (2018).
17. Yadav, S., Saha, S. & Sen, S. S. Compounds with Low-Valent p-Block Elements for Small Molecule Activation and Catalysis. *ChemCatChem* **8**, 486–501 (2016).
18. Hannah, T. J. & Chitnis, S. S. Ligand-enforced geometric constraints and associated reactivity in p-block compounds. *Chem. Soc. Rev.* **53**, 764–792 (2024).
19. Abbenseth, J. & Goicoechea, J. M. Recent developments in the chemistry of nontrigonal pnictogen pincer compounds: from bonding to catalysis. *Chem. Sci.* **11**, 9728–9740 (2020).
20. Lipshultz, J. M., Li, G. & Radosevich, A. Main Group Redox Catalysis of Organopnictogens: Vertical Periodic Trends and Emerging Opportunities in Group 15. *J. Am. Chem. Soc.* **143**, 1699–1721 (2021).
21. Moon, H. W. & Cornella, J. Bismuth Redox Catalysis: An Emerging Main-Group Platform for Organic Synthesis. *ACS Catal.* **12**, 1382–1393 (2022).
22. Planas, O., Wang, F., Leutzsch, M. & Cornella, J. Fluorination of arylboronic esters enabled by bismuth redox catalysis. *Science* **367**, 313–317 (2020).
23. Böettger, S. C., Poggel, C. & Sundermeyer, J. *ortho*-Directed Dilithiation of Hexaphenyl-carbodiphosphorane. *Organometallics* **39**, 3789–3793 (2020).
24. Buchner, M. R. et al. Di-*ortho*-beryllated Carbodiphosphorane: A Compound with a Metal–Carbon Double Bond to an Element of the s-Block. *Organometallics* **39**, 3224–3231 (2020).
25. Obi, A. D. et al. A Multidimensional Approach to Carbodiphosphorane–Bismuth Coordination Chemistry: Cationization, Redox-Flexibility, and Stabilization of a Crystalline Bismuth Hydridoborates. *Inorg. Chem.* **61**, 19452–19462 (2022).
26. Obi, A. D., Deng, C.-L., Alexis, A. J., Dickie, D. A. & Gilliard, R. J. Jr Geminal bimetallic coordination of a carbone to main-group and transition metals. *Chem. Commun.* **60**, 1880–1883 (2024).
27. Chulsky, K., Malahov, I., Bawari, D. & Dobrovetsky, R. Metallomimetic Chemistry of a Cationic, Geometrically Constrained Phosphine in the Catalytic Hydrodefluorination and Amination of Ar–F Bonds. *J. Am. Chem. Soc.* **145**, 3786–3794 (2023).
28. Kira, M., Yauchibara, R., Hirano, R., Kabuto, C. & Sakurai, H. Synthesis and X-ray Structure of the First Dicoordinate Dialkylstannylene That Is Monomeric in the Solid State. *J. Am. Chem. Soc.* **113**, 7785–7787 (1991).
29. Lay, U., Pritzkow, H. & Grützmacher, H. A second crystal modification of bis[2,4,6,-tris(trifluoromethyl)phenyl]stannylene: a stannylene (stannanediyl) dimer with weak tin–tin interactions. *J. Chem. Soc., Chem. Commun.* **260**, 262 (1992).
30. Weidenbruch, M. et al. Bis(2,4,6-tri-*tert*-butylphenyl)stannanediyl: A Diarylstannylene without Donor Stabilization. *Angew. Chem. Int. Ed.* **33**, 1846–1848 (1994).
31. Tajima, T., Takeda, N., Sasamori, T. & Tokitoh, N. A Kinetically Stabilized Stannanetellone, a Tin-Tellurium Double-Bonded Compound. *Organometallics* **25**, 3552–3553 (2006).
32. Zhao, H. et al. Cation-Triggered Stannate(II)/Stannylenoid/Stannylene Conversion. *Chem. Eur. J.* **24**, 5967–5973 (2018).

33. Khan, S., Gopakumar, G., Thiel, W. & Alcarazo, M. Stabilization of a Two-Coordinate $[GeCl]^+$ Cation by Simultaneous σ and π Donation from a Monodentate Carbodiphosphorane. *Angew. Chem. Int. Ed.* **52**, 5644–5647 (2013).
34. Katir, N., Matioszek, D., Ladeira, S., Escudié, J. & Castel, A. Stable N-Heterocyclic Carbene Complexes of Hypermetallyl Germaniu-m(II) and Tin(II) Compounds. *Angew. Chem. Int. Ed.* **123**, 5464–5467 (2011).
35. Sindlinger, C. P. & Wesemann, L. Hydrogen abstraction from organotin di- and trihydrides by N-heterocyclic carbenes: a new method for the preparation of NHC adducts to tin(II) species and observation of an isomer of a hexastannabenzene derivative [R6Sn6].*Chem. Sci.* **5**, 2739–2746 (2014).
36. Frisch, M. et al. *Gaussian16, Revision A.03* (Gaussian, Inc., 2016**)**.
37. Savin, A., Nesper, R., Wengert, S. & Fässler, T. F. ELF: The Electron Localization Fuction. *Angew. Chem. Int. Ed.* **36**, 1808–1832 (1997).
38. Bader, R. F. *Atoms in Molecules: A Quantum Theory* (Clarendon Press, Oxford, U. K., 1990).
39. Reed, A. E., Curtiss, L. A. & Weinhold, F. Intermolecular Interactions from a Natural Bond Orbital, Donor-Acceptor Viewpoint. *Chem. Rev.* **88**, 899–926 (1988).
40. Wiberg, K. B. Application of the pople–santry–segal CNDO method to the cyclopropylcarbinyl and cyclobutyl cation and to bicyclo-butane. *Tetrahedron* **24**, 1083–1096 (1968).
41. Huynh, H. V. Electronic Properties of N-Heterocyclic Carbenes and Their Experimental Determination. *Chem. Rev.* **118**, 9457–9492 (2018).
42. Gusev, D. G. Donor Properties of a Series of Two-Electron Ligands. *Organometallics* **28**, 763–770 (2009).
43. Lim, S. & Radosevich, A. T. Round-Trip Oxidative Addition, Ligand Metathesis, and Reductive Elimination in a P^{III}/P^{V} Synthetic Cycle. *J. Am. Chem. Soc.* **142**, 16188–16193 (2020).
44. Pang, Y., Leutzsch, M., Nöethling, N., Katzenburg, F. & Cornella, J. Catalytic Hydrodefluorination via Oxidative Addition, Ligand Metathesis, and Reductive Elimination at Bi(I)/Bi(III) Centers. *J. Am. Chem. Soc.* **143**, 12487–12493 (2021).
45. Bonfante, S., Lorber, C., Lynam, J. M., Simonneau, A. & Slattery, J. M. Metallomimetic C–F Activation Catalysis by Simple Phosphines. *J. Am. Chem. Soc.* **146**, 2005–2014 (2024).
46. Terrier, F. Modern Nucleophilic Aromatic Substitution (Wiley-VCH, Weinheim, 2013).
47. Gynane, M. J. S., Lappert, M. F., Miles, S. J. & Power, P. P. Ready oxidative addition of an alkyl or aryl halide to a tin (II) alkyl or amide; evidence for a free-radical pathway. *J. Chem. Soc., Chem. Commun.* **256**, 257 (1976).

Acknowledgements

This work was financially supported by the National Key R&D Program of China (2023YFC3903200), National Natural Science Foundation of China (22471176), and Natural Science Foundation of Sichuan, China (2023NSFSC1083) and the Fundamental Research Funds for the Central Universities (YJ202269). We also thank Dr. Jing Li, Dr. Dongyan Deng and Dr. Meng Yang from the College of Chemistry at Sichuan University for their suggestions and assistance in HRMS, NMR, and sc-XRD analyses. We acknowledge Dr. Hanjiao Chen and Dr. Pengchi Deng from the Analytical & Testing Center, Sichuan University for the support in EPR and NMR analyses.

Author contributions

Z.D. designed and supervised the project. Z.L. performed the synthetic experiments and analyzed the data. Y.Z. synthesized compound **1**. Z.W. and H.M. performed the computational analysis. J.Z. collected and processed the X-ray data. Z.L., Z.W., and Z.D. co-wrote the manuscript. All authors discussed the results and commented on the manuscript.

Competing interests

The authors declare no competing interests.

Additional information

Supplementary information The online version contains supplementary material available at https://doi.org/10.1038/s41467-024-54321-y.

Correspondence and requests for materials should be addressed to Zhaowen Dong.

Peer review information *Nature Communications* thanks the anonymous reviewer(s) for their contribution to the peer review of this work. A peer review file is available.